Seismic vulnerability assessment indices for buildings: Proposals, comparisons and methodologies at collapse limit states

SEISMIC VULNERABILITY ASSESSMENT INDICES FOR BUILDINGS: PROPOSALS, COMPARISONS AND METHODOLOGIES AT COLLAPSE LIMIT STATES

Sebastiano Marasco[1], Ali Zamani Noori[2], Marco Domaneschi[3*], and Gian Paolo Cimellaro[4]

[1] Postdoctoral researcher, Dept. of Structural, Geotechnical and Building Engineering, Politecnico di Torino, Italy

[2] Postdoctoral researcher, Dept. of Structural, Geotechnical and Building Engineering, Politecnico di Torino, Italy

[3*] Assistant professor, Department of Structural, Geotechnical and Building Engineering, Politecnico di Torino, Italy. *Corresponding author:* marco.domaneschi@polito.it

[4] Professor, Department of Structural, Geotechnical and Building Engineering, Politecnico di Torino, Italy

Seismic vulnerability assessment of existing buildings is an essential process for earthquake disaster management. It can support decision-makers to estimate critical response parameters and improve them. While several seismic vulnerability assessment techniques have been introduced over the past years, a detailed formulation to measure the vulnerability index of existing buildings along with the operative procedure is still lacking. Current standards and literature worldwide mostly propose simplified approaches (e.g. based on limited engineering analyses, visual inspection) to perform a rapid vulnerability assessment that can be useful when a large number of buildings should be analyzed. This paper presents a methodology to perform the seismic vulnerability assessment of existing buildings at collapse, analyzing a standard vulnerability index, and proposing alternative formulas. The methodology combines field investigations and experimental tests with nonlinear structural analyses. It has been applied to a case study that consists of an existing reinforced concrete school building to analyze and compare the proposed indices with respect to different ground motion selection procedures. Furthermore, a detailed comparison with alternative vulnerability indices from literature has been also performed.

KEYWORDS

Earthquake, existing buildings, vulnerability index, nonlinear analysis, field investigations.

INTRODUCTION

The seismic vulnerability assessment of existing buildings is an essential step for earthquake disaster management that allows to optimize resources allocation, provide a fast response after a disaster, and mitigate consequences of earthquakes(Cockburn and Tesfamariam 2012). The "seismic vulnerability" is defined as the "susceptibility of a population of buildings to undergo damage due to seismic ground motion"(Alam, Alam, and Tesfamariam 2012; Hill and Rossetto 2008; FEMA1999 1999; Cockburn and Tesfamariam 2012) and it depends on several key parameters such as the seismic hazard level, the quality of the constitutive materials, the building age, the level of maintenance, the building archetype(Bertogg, Hitz, and Schmid 2002), etc. However, often this information might not be available. Furthermore, the scale of observation is an important element in vulnerability assessments. Indeed, the spatial scale of analysis implies the selection of certain structural details which are more refined for individual building-scale. On the contrary, urban and regional-scale of observation require higher computational effort which entails the use of typological building data. In the following, the state of the art of existing methods for the vulnerability assessment of buildings has been reported, also making reference to the current standards.

In the literature, different methods for seismic vulnerability assessment have been proposed(Calvi et al. 2006; Okada and Takai 2000; Guéguen, Michel, and LeCorre 2007; Spence et al. 2008; Lang and Bachmann 2004; Sucuoğlu, Yazgan, and Yakut 2007; Martinelli et al. 2008). They can be classified into two main categories: empirical and analytical. However, both categories can be merged in hybrid approaches(Calvi et al. 2006; Colombini 2014). Empirical methods allow evaluating seismic vulnerability by correlating seismic intensity with the level of observed damage (statistical approach), while analytical approaches use mechanical models that reproduce the main characteristics of buildings and estimate the capacity of the structure(Noori et al. 2017) and the demand level imposed by an earthquake scenario (quantitative approach)(Chácara et al. 2019; Khan et al. 2019; Lorenzoni, Valluzzi, and Modena 2019; Djemai, Bensaibi, and Zellat 2019; Chieffo et al. 2019; Gentile et al. 2019; Giordano,

De Luca, and Sextos 2020; Yakut, Ozcebe, and Yucemen 2006). Vulnerability assessment may be also addressed based on simple evidence without significant calculation or modeling (qualitative approach). An example of a qualitative approach is given by the Rapid Visual Screening (RVS) procedures that require a visual evaluation and limited information on the building under study; therefore, they are classified as First Level procedures. Among the others, Islam et al. (2017) proposed a simplified vulnerability index based on the rapid screen evaluation of the existing Reinforced Concrete (RC) buildings' capacity using data from past earthquakes. The seismic vulnerability index was evaluated as the ratio between the average lateral load-carrying capacity and the mean shear stress on the resistant members. (Perrone et al. 2015) proposed an RVS method for evaluating the safety index for hospital buildings. The methodology was tested on two hospitals located in different seismic areas of Italy. Later, (Ruggieri et al. 2020) developed an RVS methodology to assess the seismic risk of RC school buildings. The vulnerability was assessed through a survey, while the hazard and exposure data were also taken into account. Although RVS methods provide a quick evaluation of the seismic building vulnerability, they are addressed at identifying those structures that require further technical investigation(Jain et al. 2010).

Second Level procedures require limited engineering analyses based on the site measurement, structural drawings, and visual inspection data(Sinha and Goyal 2004). Several simplified vulnerability assessment methods of existing buildings have been carried out during the last two decades. Thermou and Pantazopoulou (2011) proposed a vulnerability assessment method for existing RC buildings under the design earthquake. They estimated the inter-story drift from the period of the structure by relating the structural stiffness to the area ratio of the vertical elements. Asteris et al. (2014) presented a methodology to evaluate the seismic capacity of masonry buildings using case studies from historical masonry structures in the European area. Later on, Formisano and Marzo (2017) assessed the seismic vulnerability of a masonry building that was damaged during the 2012 central Italy earthquake. They proposed a simplified method following the instruction provided by the Italian Guidelines on Cultural Heritage. Uma, Dhakal, and Nayyerloo (2014) used a displacement-based method to carry out the vulnerability assessment of Christchurch buildings following the 2012 earthquake event. They used the data from the building safety evaluation surveys to determine the damage level. The observed damages were linked with drift limit states adopted in the theoretical approach. Focusing on reinforced concrete (RC) structures, Kassem, Nazri, and Farsangi (2019) proposed a simplified method modifying the existing Italian and European Macro-seismic approaches.

Third Level assessment procedures require detailed information on the structure and use refined computer methods and analyses. El Khoudri et al. (2016) developed a numerical method to evaluate the seismic vulnerability using incremental dynamic analysis to predict the distribution of expected losses due to an earthquake event. However, the proposed approach does not provide an explicit formulation of a vulnerability index but instead employs nonlinear dynamic analysis for the construction of fragility curves. The study developed by Emami and Halabian (2017) aims at establishing fragility relationships as well as collapse probability of high-rise RC core-wall buildings under maximum considered earthquake ground motions using the Incremental Dynamic Analysis (IDA) and multi-directional pushover analysis. Also this study, focused on the structural typology of tall buildings, is not focused on the formulation of a vulnerability index, but on the probabilistic assessment of the collapse through fragility analysis. In some cases, third-level analyses can be used to extract general information related to a group of buildings. These methodologies aim at providing useful information which can be adopted in second-level methodologies. (Ruggieri et al. 2021) performed both static and dynamic nonlinear analyses on a sample of 15 low-rise existing school buildings to assess the associated fragility curves. The proposed methodologies revealed satisfactory results for both individual building-level and regional fragility curves. (Calvi, Priestley, and Kowalsky 2007) proposed an alternative Displacement-Based Assessment (DBA) that relates the structural vulnerability to the deformations instead of the forces. The effectiveness of the DBAs was analyzed by (Gentile, Nettis, and Raffaele 2020) to investigate their practical applications. Both static and dynamic DBAs were adopted in the analysis of a set of 36 RC continuous-deck bridges with different span numbers, pier heights, and transverse stiffness. The New Zeland Society for Earthquake Engineering (NZSEE 2017) recommends the use of DBAs that can be based on several analysis procedures to assess the structural capacity. The results of the seismic performance of single structures are then computed as capacity/demand ratio.

Most building codes in the world implicitly propose different seismic vulnerability assessment methods. RVS is the simplest method introduced by FEMA154 (2002). It is based on performing basic structural computations for a quick evaluation of building portfolios in large areas (Harirchian and Lahmer 2019). However, it does not require performing a detailed seismic analysis of individual buildings. Accordingly, buildings are classified into two categories using cutoff scores performing sidewalk surveys: (*i*) those acceptable for life safety level of performance

or (*ii*) seismically unsafe. Based on this classification, the final needs for rehabilitation can be determined. Later on, the National Research Council of Canada (1993) introduced a final cutoff score following the procedure provided by FEMA154 (2002) for both structural and non-structural components. It also takes into account the building occupancy class and its importance. Upon the computed score, the appropriate rehabilitation strategy can be made. FEMA310 (1998) improved the RVS method by proposing a three-tiered procedure, in which Tier 1 is the screening phase in the form of checklists for a fixed performance level. Tier 2 and Tier 3 are performed where the outcome of Tier 1 is too conservative or a significant economic advantage was verified. Eurocode-8 (2005) provides criteria for the seismic vulnerability assessment of existing buildings incorporating a *model uncertainty factor* to include uncertainties related to the analysis. The New Zealand Guidelines (NZSEE-2003 2014) proposes the visual screening procedure of ATC-21 (1988) and computes the final building vulnerability score by aggregation of fourteen structural indicators that are representative of the potential building's damage components. Recently, the new Italian standard (NTC2018 2018) introduced a method to compute the seismic vulnerability index of existing buildings based on the bearable maximum seismic action. In previous codes, the attention was focusing on the structural verification to withstand an assigned level of seismic demand, while the new Italian code is converging toward the performance level of the building (Naeim, Bhatia, and Lobo 2001). However, it does not provide any specific procedure for the computation of the maximum bearing capacity (NTC2018 2018).

The previously mentioned studies and guidelines on the vulnerability assessment of existing buildings made meaningful advancements in this field of research considering a wide class of conditions and building typologies. However, they do not provide much knowledge on the formulation of specific vulnerability indices for existing buildings, proposing an accurate step-by-step procedure that includes field tests with nonlinear structural analyses (Third Level procedures). On the contrary, this contribution explores these aspects and proposes different indices to quantitatively measure the building vulnerability starting from the new Italian seismic provision. This paper proposes three methods for assessing the vulnerability index with application to a real case study building. The effects of different factors that may affect the computation have been addressed: type of analysis (nonlinear, static or dynamic), collapse drift threshold, record selection, Intensity Measure (IM) parameter for the seismic action. The results are then compared with those obtained through existing alternative first and second-level approaches, while the influence of the motion selection in evaluating the building capacity is also investigated.
The proposed methods to assess the vulnerability indices include both practical approaches such as pushover analysis and more refined approaches through nonlinear time history analyses. Furthermore, the paper provides also comparisons and discussion about the different methodologies that may be useful for engineering practice.

METHODOLOGIES FOR SEISMIC VULNERABILITY ASSESSMENT

The seismic vulnerability of an existing building depends on different conditions such as aging, poor maintenance, outdated design, materials' characteristics, the construction place, and natural events, etc. According to the current Italian standard(NTC2018 2018), the seismic vulnerability index for an existing building is defined by a new parameter ζ_E that is the ratio between the maximum bearable seismic action of the existing structure and that one required to design a new one on the same site with the same dynamic properties(CIRCOLARE 2019). The Peak Ground Acceleration (*PGA*) is used to define this index. This section explores the standard vulnerability index and compares it with alternative formulations.

Vulnerability index- Method #1

The seismic vulnerability index for existing buildings as introduced by the current Italian code(NTC2018 2018) is based on Equation (1):

$$\zeta_E = \frac{PGA_{collapse}}{PGA_{design}} \tag{1}$$

where $PGA_{collapse}$ is the maximum bearable seismic action of the existing structure in terms of PGA, while PGA_{design} is the peak ground acceleration to design a new building with the same characteristics as the existing one. Despite Equation (1) is consistent with the Italian code prescriptions, an alternative procedure is herein proposed to assess the terms of the equation. Within Method #1, the $PGA_{collapse}$ value is determined through performing nonlinear dynamic analyses using an iterative procedure. With reference to a multi-story building, first, the maximum inter-

story drift $\delta_{collapse}$ associated with the collapse state of the structure is defined. Second, a set of seven records compatible with the design spectrum is selected and the structural response in terms of inter-story drift is computed. The average maximum inter-story drift $\delta_{\max}$ is compared with $\delta_{collapse}$. Afterward, if $\delta_{\max}$ is less than $\delta_{collapse}$, the time histories are scaled using the PGA until the average maximum inter-story drift reaches $\delta_{collapse}$. At this stage, the $PGA_{collapse}$ in Equation (1) is computed as the average PGA of the seven scaled time histories.

The flowchart in Figure 1 summarizes the procedure to evaluate the seismic vulnerability index for Method #1 starting from the field investigations block. The FE model is prepared and calibrated using the information of the on-site investigations.

Vulnerability index- Method #2

An alternative formulation to compute the vulnerability index is herein proposed in Equation (2):

$$\zeta_E = \frac{S_a}{S_{a,d}} \tag{2}$$

where S_a is the maximum bearable spectral acceleration of the existing building at the reference period of the structure that corresponds to the elastic first mode period, while $S_{a,d}$ is the spectral acceleration that should be used to design a new building with the same characteristics at the same site. The S_d value is determined by the design spectrum for the considered hazard level (HL), whereas S_a parameter is computed performing nonlinear dynamic analyses. The inter-story drift $\delta_{collapse}$ is determined following the procedure of Method #1. Then, a set of spectrum compatible time histories is selected. The mean value $\delta_{\max}$ of the seven maximum inter-story drifts obtained by the analyses is computed and compared with $\delta_{collapse}$.

Conversely to Method #1, when $\delta_{\max}$ is less than $\delta_{collapse}$, a new set of ground motion records is selected based on the scaled design spectrum. This procedure is repeated until $\delta_{\max}$ is equal to $\delta_{collapse}$. When this condition is verified, the corresponding S_a in Equation (2) is determined, computing the mean value of the seven spectral accelerations at the reference period of the structure that corresponds to the elastic first mode period. The flowchart in Figure 2 summarizes the methodology of Method #2, where the main difference with respect to Method #1 is that S_a is used instead of the *PGA*, and the ground motions selection is repeated at each iteration.

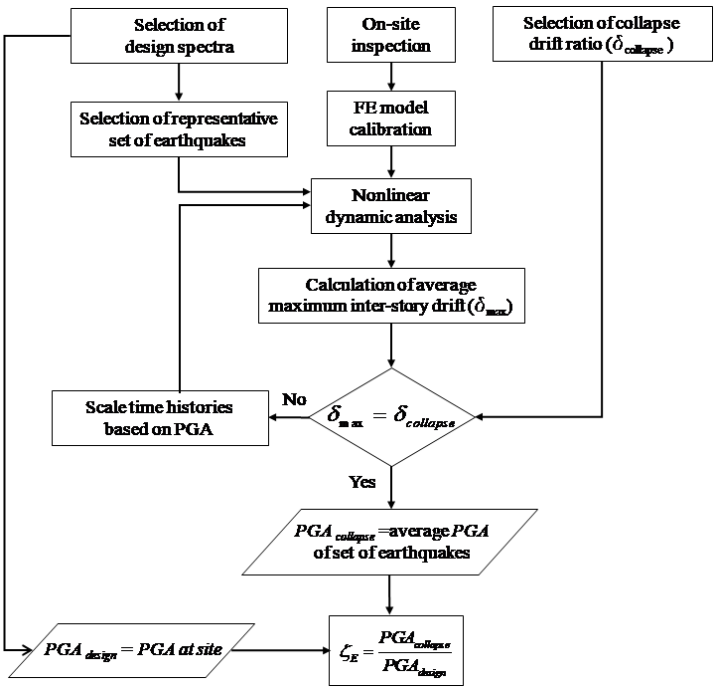

Figure 1 Flowchart to compute vulnerability index based on Method #1.

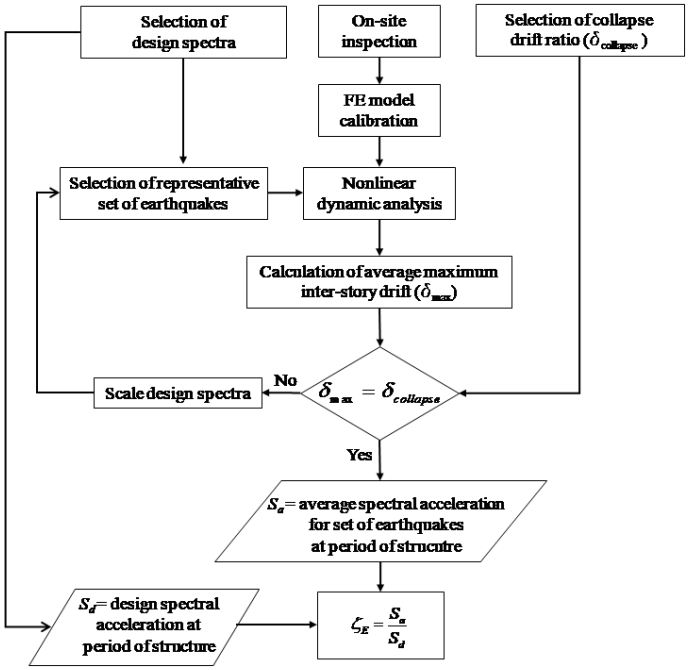

Figure 2 Flowchart to compute vulnerability index based on Method #2.

Vulnerability index- Method #3

An alternative formulation to compute the vulnerability index performing nonlinear static analysis is proposed in Equation (3):

$$\zeta_E = \frac{F^*_{collapse}}{F^*_{\max}} \tag{3}$$

where $F^*_{collapse}$ is the bearable maximum base shear of the building computed through pushover analyses; $F^*_{\max}$ is the force associated with the performance point of the structure. $F^*_{collapse}$ corresponds to the maximum base shear that the structure can withstand as shown in Figure 3. Instead, $F^*_{\max}$ value can be computed using one of the methods presented in NTC2018 (2018) such as the Capacity-Spectrum Method (ATC-40 (1996)) or the N2 Method (Fajfar and Gašperšič 1996) (Figure 3). Figure 4 summarizes the flowchart of the procedure.

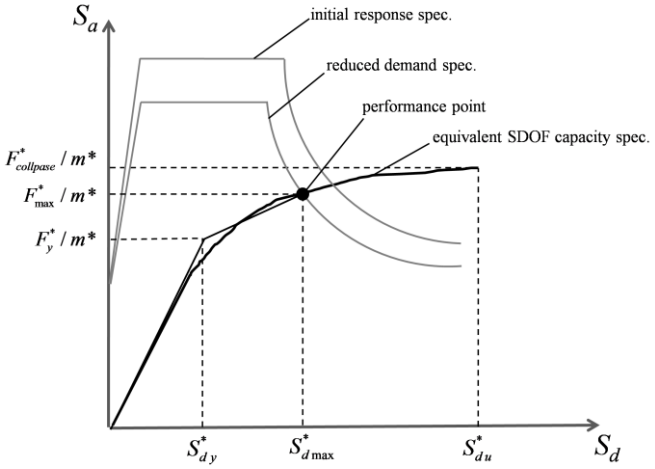

Figure 3 Identification of performance point (adapted from NTC2018 (2018)).

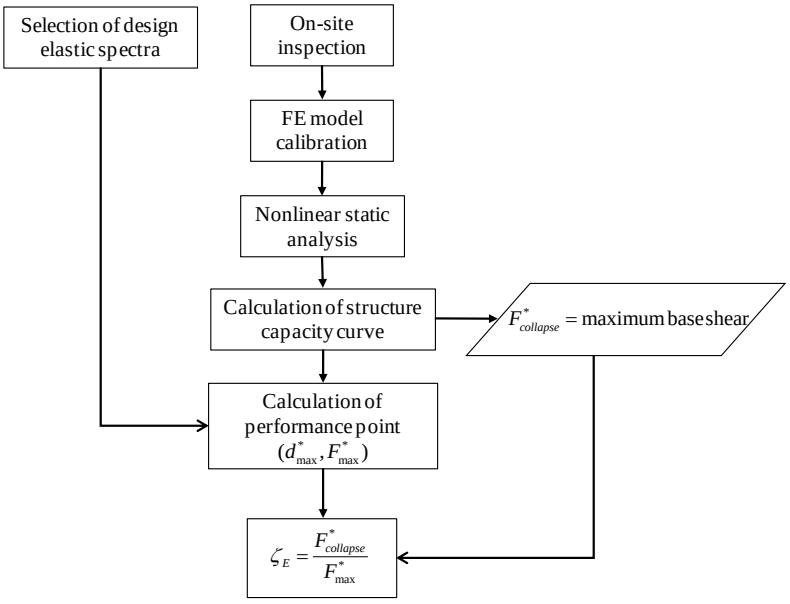

Figure 4 Flowchart to compute vulnerability index based on Method #3.

CASE STUDY

An existing school building located in Northern Italy has been used as a case study to compare the three proposed vulnerability assessment indices. The building is an RC structure with shear walls in both principal directions. Two types of columns cross-sections have been used (0.35x0.40 and 0.40x0.40 m) with a mean compressive strength of 31.5 MPa. A steel reinforcement ratio of about 1.5 % has been adopted. The horizontal deck is made by reinforced brick-concrete slab at each floor level. The building was designed in the early '60s with outdated standards (without specific prescriptions on seismic actions) and built in 1967. It consists of three main blocks: the lateral blocks (A and C) that host classes and the central block (B) that hosts staircases and connects the two lateral blocks (Figure 5a). The structure is classified as polar symmetric in plan and regular in elevation with a total height of 13.65m (Figure 5b). The building is located on soil type D (soft soil) with reference shear wave velocity ranging from 100 m/s to 180 m/s according to NTC2018 (2018). The building design category corresponds to Class IV representing strategic buildings such as schools. The geometrical data have been extracted by the existing BIM model recently prepared by the municipality (Figure 5a).

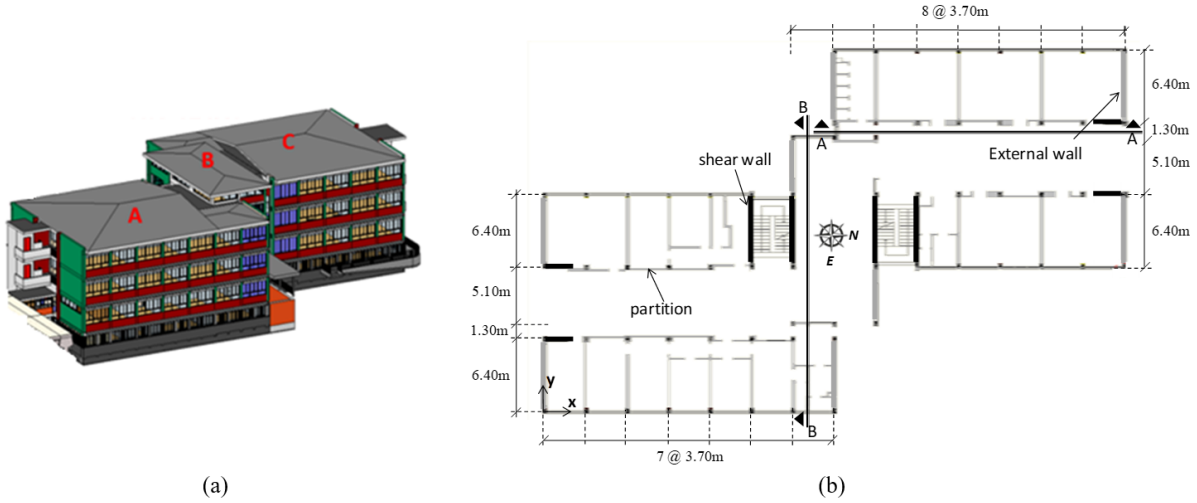

Figure 5 BIM model (a), and plan view (b) of the case study building.

Ambient Vibration Tests (AVTs) have been performed to detect the modal characteristics of the building, to calibrate the FE model. In detail five tri-axial Force Balance (FB) accelerometers (numbered from #50 to #54) (Figure 6) have been used. The sensors are low noise (2.5 μg/√Hz) accelerometers with a dynamic range of 160 dB equipped with GPS receiver and WiFi communication to create a local synchronized wireless network.

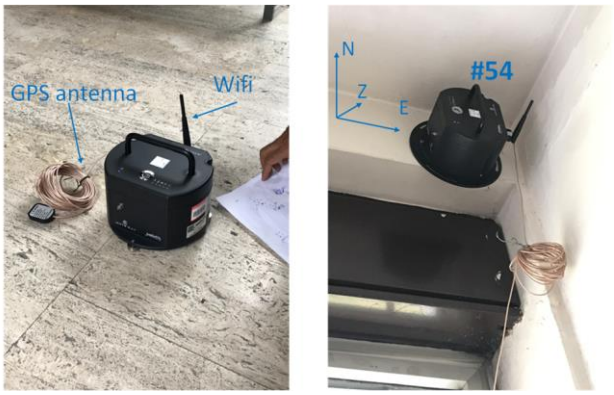

Figure 6 Force balance accelerometer for ambient vibration tests (#54 for C1 configuration).

Different sensor configurations have been designed to identify the translational and torsional modal characteristics of the building. In total, seven sensor configurations have been used: three for the identification of global behavior (G1-G3) and four (C1-C4) for the local behavior. Figure 7 exemplifies the position of sensors for G1 and C1 configurations. Each test had a duration of about 15 minutes with a 200Hz sampling rate.

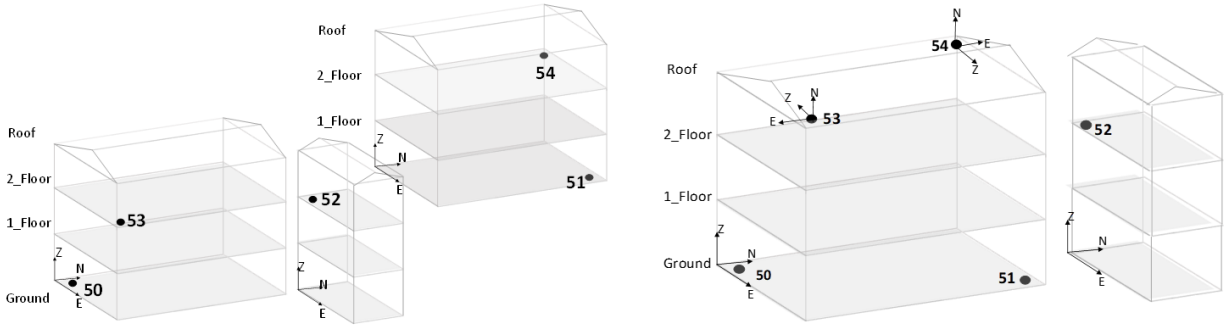

Figure 7 Accelerometer configuration for ambient vibration test: global_G1 (a) and local_C1 (b).

Output-only methods have been used to analyze the experimental data and to identify the building dynamic characteristics such as the natural frequencies and the modal shapes (Cimellaro, Piantà, and De Stefano 2012). The raw recorded signals corresponding to each configuration have been extrapolated using a low-pass filter setting the cut-off frequency at the value of 20Hz. The resulting signals have been processed through Frequency Domain Decomposition (FDD) and Random Decrement Technique (RDT) using Matlab codes (MATLAB 2017). The singular values diagram of the PSD matrix as a function of frequencies has been computed, as well as the Cross Power Spectral Density (CPSD) matrix through the CPSD function. The graphic representation of the singular spectrum allows identifying the peaks corresponding to the main natural frequencies of the building in each direction. Figure 8a and Figure 8b show the Singular Values (SV1, SV2, and SV3) of the PSD matrix obtained through the RDT for G1 configuration in East and North directions, respectively.

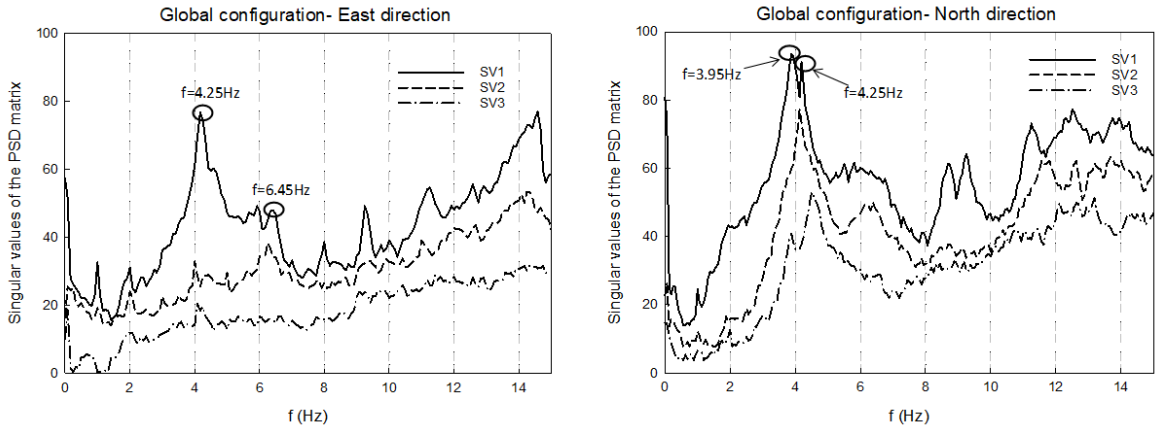

Figure 8 Identified singular values of the PSD matrix using the RDT method for G1 configuration in East (a) North (b) directions.

Table 1 lists the building natural frequencies identified through FDD and RDT techniques. The same identified frequencies in both East and North directions can be associated with a torsional or translational mode along the diagonal direction (N-W). Table 1 shows that the frequencies obtained with the two algorithms are reasonably equivalent. The first dominant mode is in the North direction with a period of 0.26 s. The second mode is a torsional mode with a period of 0.24 s, while the third mode is a translational mode in the East direction with a period of 0.16 s. As expected, the result shows that the structure is stiffer in the transversal direction (East) since the stiffness associated with the shear walls is greater in that direction with respect to the longitudinal one (Figure 5b).

Table 1 Identified natural frequencies.

Mode	Direction	FDD [Hz]	RDT [Hz]	FEM [Hz]
First	North	3.95	3.89	3.84
Second	Torsional	4.25	4.19	4.22
Third	East	6.45	6.44	6.45

A FE model (Figure 9a) has been developed (CSI 2018) and calibrated to reproduce the dynamic behavior of the school building. Non-destructive tests have been performed to assess the material characteristics for the main structural elements. In detail, the rebound hammer test has been used to estimate the concrete elastic modulus and strength characteristics, while the pachometer has been used to identify the concrete cover conditions and the steel reinforcement details. The mean value of 31.5 MPa has been used as concrete strength for beams, columns, and shear walls. According to many international standards destructive tests are mandatory to evaluate the compressive strength of concrete members because the hammer rebound test could lead to overestimation of the concrete compressive strength. However, for the purposes of this study, this aspect is not essential.
A thermal camera (FLIR E6) has been used to detect secondary structural elements that were not reported in the available technical drawings and the BIM model. Therefore, the geometry of the structural members has been imported from the available detailed BIM model and confirmed by the onsite technical inspections. The strength and elastic modulus of the tested members have been set to match the hammer test results, while the elastic coefficients of the remaining structural elements, their stiffness contributions, and additional nonstructural masses have been identified to match the first three modal shapes and periods (Table 1).

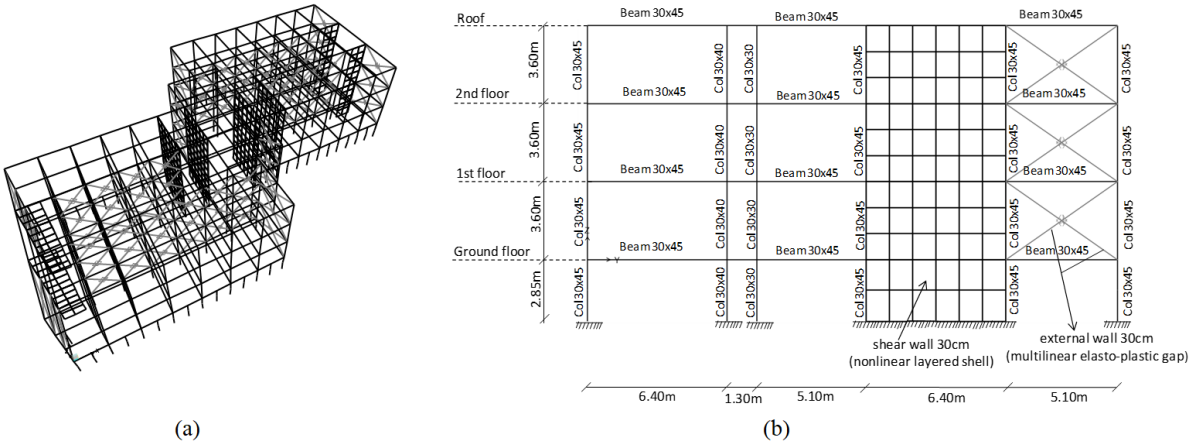

Figure 9 FE 3D model (a), and frame view B (b) of the case study building.

Beams and columns have been modeled as frame elements, while the nonlinear layered shell has been used to model the shear walls (Figure 5). The frame nonlinearities have been introduced by defining P-M2-M3 and M3 plastic hinges for columns and beams, respectively (ASCE-7 2014). Besides, the nonlinear GAP element has been used to model external walls and partitions. Its initial stiffness has been computed using the Equivalent Strut Model proposed by Al-Chaar (2002). The bilinear elastic-plastic curve has been defined to take into account the masonry wall's nonlinear behavior based on the Idealized Force-Deflection Relation described in FEMA273 (1997). The columns have been assumed to be fixed at the base, while a rigid body behavior has been assumed for each floor diaphragm. The FE model has been developed using SAP2000 (CSI 2020). A 5% Rayleigh damping has been considered, while a concentrated plasticity model (FEMA356 2000) (type P-M2-M3 for columns and beams) has been chosen to take into account the nonlinearity in the structural components. The length of each plastic hinge has been fixed to 5% of the structural member length. The beam-column joint stiffness has been modeled through rigid links which ensure a perfectly rigid connection between the structural members in the related overlapped zones. The hysteretic behavior is reproduced by Takeda (Takeda, Sozen, and Nielsen 1970) model. The shear walls have been

modeled using *Shell – Layered/Nonlinear* elements where two external confined concrete layers and one inner unconfined concrete layer have been modeled. A 3% of reinforcement has been used to model the confined layers, while a 0.4% has been assumed for the unconfined layer. Furthermore, the thickness of the confined layers has been set equal to 15% of the shear wall length. The beam-shear wall joints have been modeled by releasing the rotational degree of freedom of the beam element. This assumption allows transferring only shear forces to the shell elements which do not bear in-plane rotation. Finally, the infill walls have been modeled as *gap* elements that bear compression only along their axes. Each gap element connects the upper joint of a column to the lower joint of the adjacent column. The equivalent stiffness of each element has been assumed based on the Al Char method (Al-Chaar, Issa, and Sweeney 2002), where an equivalent compressive strength of 3.5 MPa has been considered for the infill walls. The diagonal strength of each element has been reduced based on the measure opening percentage of each infill. The final results in terms of frequencies of the calibrated FE model are also shown in Table 1.

Remarks on the numerical analyses

Methods #1 and #2 employ dynamic nonlinear time history analyses to estimate the global building response, and a set of seven spectrum-compatible real ground motions in each principal direction is used as seismic input. The mean seismic response and its dispersion depend on the record-to-record variability caused by (*i*) the definition of the limit state and the Engineering Demand Parameters (EDPs), (*ii*) the considered seismic Intensity Measure (IM), and (*iii*) the selected set of ground motions(Adam et al. 2014).

The dynamic response variability related to the definition of the limit states *(i)* is herein taken into account by assuming two thresholds of inter-story drift associated with the collapse Damage State ($\delta_{collapse}$). The first one is 2% drift limit that corresponds to concrete buildings with shear walls according to FEMA273 (1997), while the second one is 0.8% that corresponds to non-ductile reinforced concrete with squat walls according to Ghobarah (2004). About the choice of the IM parameters *(ii)*, the PGA and the maximum spectral acceleration at the reference period of the structure (*Sa(T)*) are assumed in Methods #1 and #2, respectively. The first one reflects the standard requirements, while the second has been herein proposed as an extension of Method #1. Finally, to cope with the variability in the dynamic response associated with the set of records *(iii)*, three different Ground Motion Selection and Modification (GMSM) procedures are used.
The energy-based GMSM method proposed by Marasco and Cimellaro (2018) is first adopted as the reference procedure for selecting a set of seven real ground motions in both horizontal directions. The procedure aims at comparing a set of horizontal ground motions at various frequency ranges with the target frequency content (Marasco and Cimellaro 2017). This approach deals with reducing the scatter of the structural response parameters while preserving the median demand. In the numerical analysis on the school building case study, OPENSIGNAL software (Cimellaro and Marasco 2015) is used to define seven pairs of horizontal records from NGA-West2, European Strong Motion Database (ESMD), and the Italian strong motion database (previously named as ITACA).
A suite of seven motions is also generated in agreement with the recently released Italian seismic code (NTC2018 (2018)) and Eurocode-8 (2005) by using the REXEL software(Iervolino, Galasso, and Cosenza 2010). The objective function used in the ground motion search is the mean deviation of the record's spectra with respect to the target spectrum in the reference period range (Eq.(4)).

$$OF = \sqrt{\frac{1}{N} \cdot \sum_{i=1}^{N} \left(\frac{Sa_j(T_i) - Sa_s(T_i)}{Sa_s(T_i)} \right)^2} \tag{4}$$

where $Sa_j(T)$ and $Sa_s(T)$ are the spectral acceleration of the jth record at the period T_i and the target spectral acceleration at the same period T_i, respectively. The coefficient N represents the number of sampled points of the spectrum. The software performs GMSM within the ESMD, while aiming at selecting a set of seven ground motions that minimize the objective function given by Eq.(4).
Finally, seven horizontal motions are selected in compliance with the ASCE-7 (2014) through the QuakeManager integrated tool (Hachem 2008) and using the geometric mean of the record's spectral accelerations with respect to the target as the objective function. The set of seven ground motions are selected from the NGA-West2 database.

Results - Method #1

The $PGA_{collapse}$ is evaluated through the iterative procedure summarized in Figure 1 performing Nonlinear Time History Analyses (NTHA). First, a hazard level (HL) with a 5% probability of exceedance in 50 years has been defined corresponding to the Limit State of Collapse (LSC) (NTC2018 (2018)). Seismogenic characteristics have been also assessed according to the de-aggregation study at the site (available at the link: http://esse1-gis.mi.ingv.it/) providing the maximum and minimum values of magnitude and source-to-site distance representative of the seismic site hazard.

A set of seven real ground motions in both horizontal directions has been selected using the three assumed GMSM procedures described at the previous section, while considering the LSC horizontal design spectrum at the reference site of Melzo (Italy: Lat. 9.4263, Long. 45.5022) as the target spectrum. Since the building is regular, the first period has been selected as the conditioning period (T_{ref} = 0.26 s) for the spectrum compatibility criterion. The PGA has been assumed as the IM parameter, while the period range 0.052-0.52 s has been considered for the spectrum compatibility process.

The seven pairs of motions selected through the three assumed GMSM methods and the related mean spectra are reported in Figure 10 for both horizontal directions. The two ground motion components (N-S and E-W) of the record that respects the spectrum compatibility will be selected. The mean spectrum compatibility with the design spectrum at the reference period range [$0.2T_{ref}$- $2T_{ref}$] has been set as the objective criterion in the ground motion fitting procedures. In all the cases, the mean spectrum compatibility within the range [$0.2T_{ref}$ - T_{ref}] is satisfactorily respected. The percentage difference between the design spectrum and the average ground motion spectrum is about 8.2%, 11.8%, and 10.5%, for Marasco and Cimellaro (2018), Iervolino, Galasso, and Cosenza (2010) and Hachem (2008) method, respectively. These values are evaluated as the average of the percentage differences calculated in the spectrum-compatibility period. On the other hand, for periods greater than T_{ref} the mean spectrum shows a higher deviation from the target spectrum.

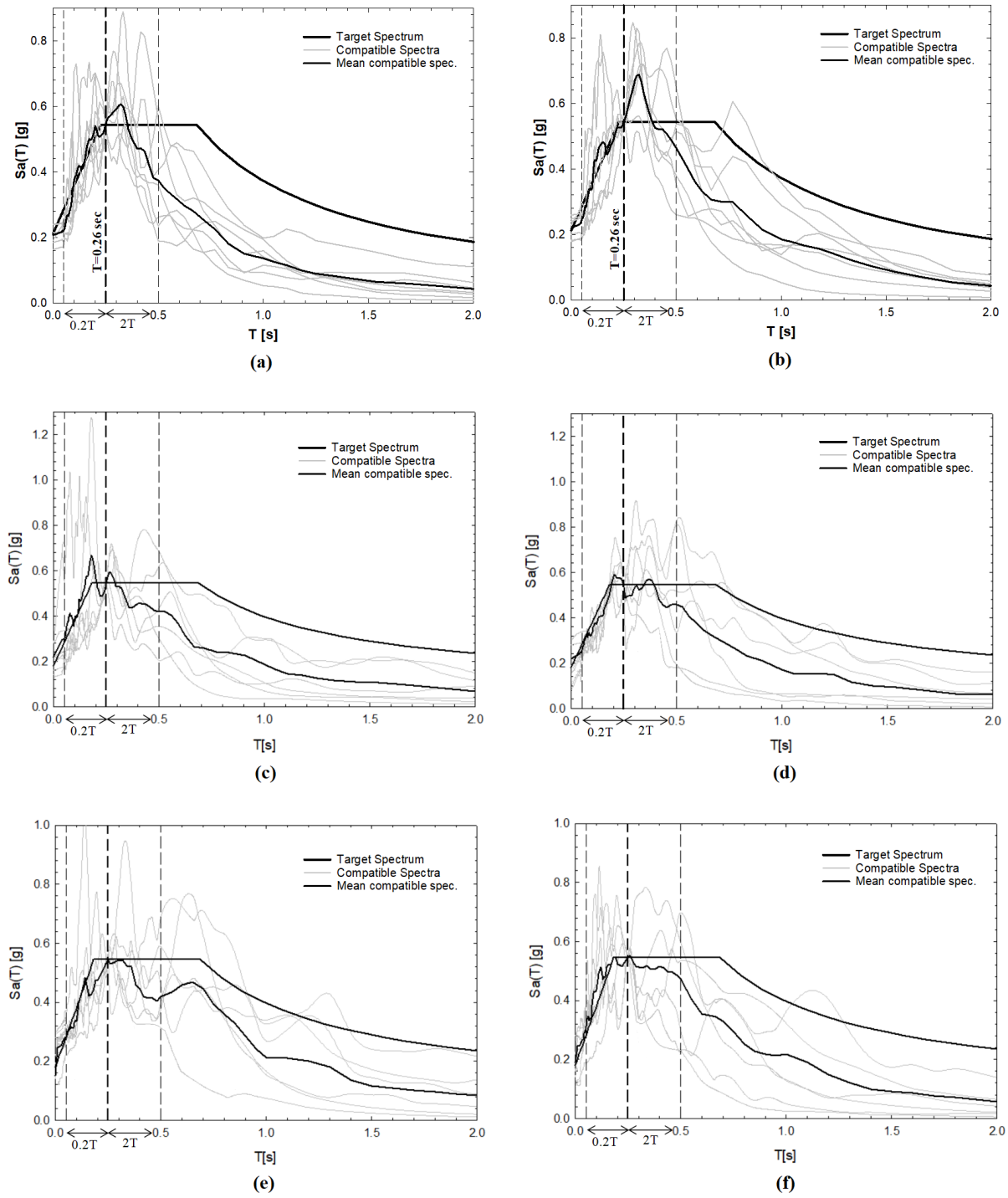

Figure 10 Design spectrum, mean spectrum, and set of seven compatible spectra obtained with Marasco and Cimellaro (2018) in x (a) and y (b) directions, Iervolino, Galasso, and Cosenza (2010) in x (c) and y (d) directions, and Hachem (2008) in x (e) and y (f) directions.

NTHAs have been performed to identify the $PGA_{collapse}$ value by applying time histories simultaneously in both horizontal directions. Therefore, the dynamic response of the building in terms of the mean maximum inter-story drift of the seven records has been computed and compared with $\delta_{collapse}$. If it is lower than $\delta_{collapse}$ the records have been scaled until the mean of the maximum inter-story drift reaches $\delta_{collapse}$. At that iteration, the $PGA_{Collapse}$ value

has been identified as the average of the PGAs of the seven scaled records while the associated standard deviation ($\beta_{collapse}$) has been considered as a variability index of the dynamic response. Table 2 presents the computed $PGA_{Collapse}$ values and the related vulnerability indices obtained through the three considered GMSM approaches.

Table 2 Vulnerability indices computed using Method #1.

Drift limit ratio	PGA_{design}	Marasco and Cimellaro (2018)			Iervolino, Galasso, and Cosenza (2010)			Hachem (2008)		
		$PGA_{collapse}$	$\beta_{collapse}$	ζ_E	$PGA_{collapse}$	$\beta_{collapse}$	ζ_E	$PGA_{collapse}$	$\beta_{collapse}$	ζ_E
[%]	[g]	[g]	[g]	[-]	[g]	[g]	[-]	[g]	[g]	[-]
0.8 % (Ghobarah 2004)	0.215	0.262	0.02	1.22	0.280	0.03	1.30	0.258	0.03	1.27
2 % (FEMA 273)	0.215	0.302	0.03	1.40	0.327	0.05	1.52	0.316	0.04	1.47

As expected, the result shows that the vulnerability index using the 2.0% drift limit as a control parameter is always higher than the ones computed using 0.8% threshold. This difference depends on the strength and the ductility of the structural system.

Results - Method #2

The design spectral acceleration $S_{a,d}$ at the reference period of the structure (T_{ref}=0.26 s) for the LSC is equal to 0.544g (Figure 10). The maximum bearable spectral acceleration S_a has been estimated through the iterative procedure in Figure 2 setting the adopted inter-story drift limits ($\delta_{collapse}$ = 0.8 and 2%). Differently from Method #1, instead of scaling records based on PGA, a set of seven new records has been selected at each iteration by scaling the design spectrum. The procedure has been repeated until the mean of the maximum inter-story drift $\delta_{\max}$ reached $\delta_{collapse}$. The three adopted GMSM procedures have been used to select the seven pairs of ground motions in both horizontal directions.

For sake of simplicity, only the mean spectra of the final seven records at collapse state for 0.8% drift limit associated with the three considered GMSM approaches have been illustrated in Figure 11.

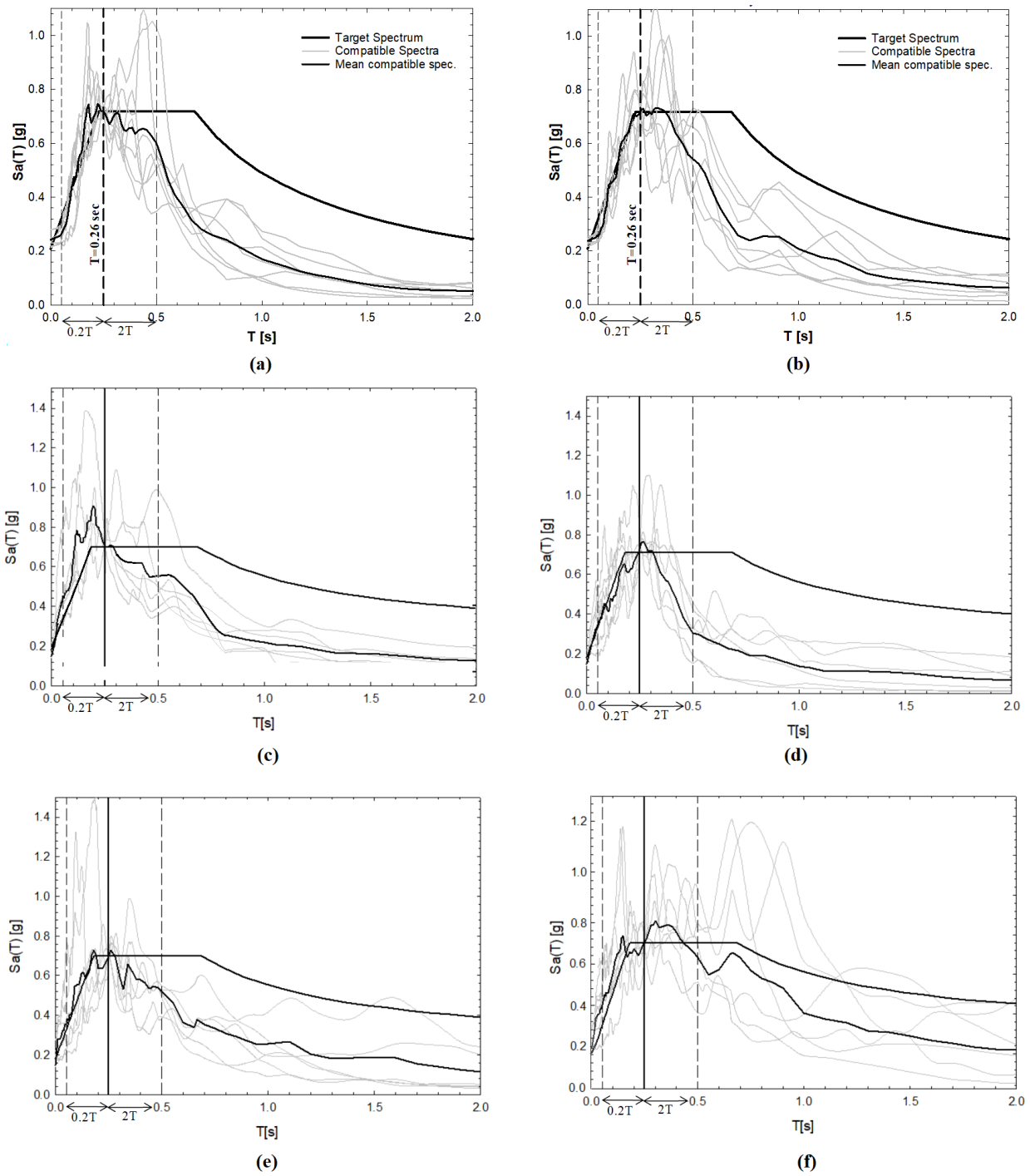

Figure 11 Scaled design spectrum, mean spectrum, and set of seven compatible spectra obtained with Marasco and Cimellaro (2018) in x (a) and y (b) directions, Iervolino, Galasso, and Cosenza (2010) in x (c) and y (d) directions, and Hachem (2008) in x (e) and y (f) directions, for 0.8% drift limit.

Table 3 shows the maximum bearable spectral accelerations S_a and the corresponding vulnerability indices. Again, as expected, the computed vulnerability indices using the 2.0% drift limit as the control parameter are always higher than those computed using the 0.8% drift limit for all the considered GMSM procedures.

Table 3 Vulnerability indices computed using Method #2.

Drift limit ratio	S_d	Marasco and Cimellaro (2018)			Iervolino, Galasso, and Cosenza (2010)			Hachem (2008)		
		S_a	$\beta_{collapse}$	ζ_E	S_a	$\beta_{collapse}$	ζ_E	S_a	$\beta_{collapse}$	ζ_E
[%]	[g]	[g]	[g]	[-]	[g]	[g]	[-]	[g]	[g]	[-]
0.8 % (Ghobarah 2004)	0.544	0.718	0.04	1.32	0.688	0.06	1.27	0.728	0.04	1.33
2 % (FEMA 273)	0.544	0.861	0.05	1.58	0.844	0.08	1.55	0.877	0.06	1.61

The computed vulnerability indices for Method #2 have been checked by using PGA values instead of S_a, assuming the collapse threshold and using the Marasco and Cimellaro (2018) GMSM approach. In this case, the vulnerability index assumes a lower value (1.17). This result is mainly driven by the record selection that is performed each time the spectrum is amplified. Indeed, the selection criteria is based on the target period of the building, while more variability characterizes the PGA.

Results - Method #3

The expected seismic performance of the building has been finally evaluated using nonlinear static analyses (Figure 4). Uniform and fundamental mode proportional load patterns have been used in both x and y directions to assess the capacity curve of the case study building (Figure 12).

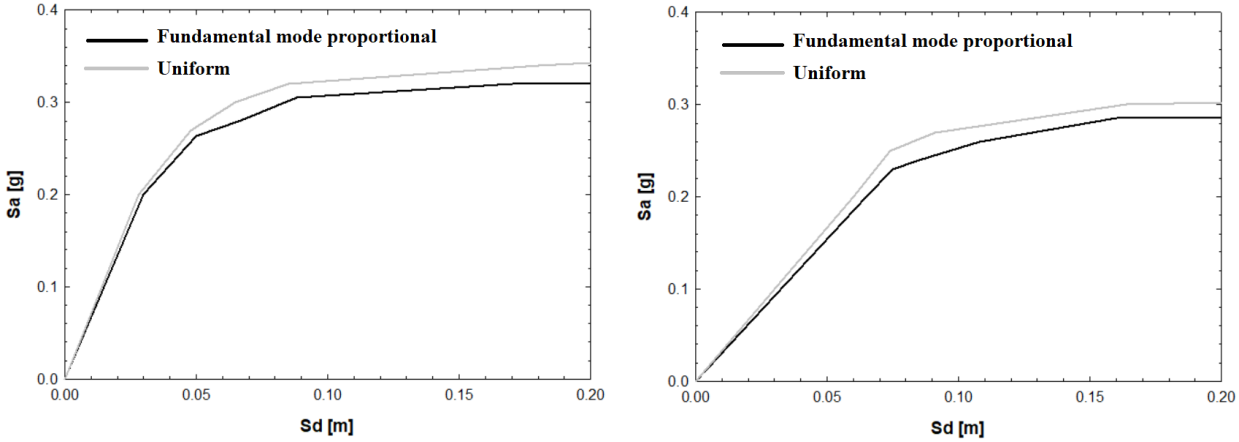

Figure 12. Capacity curves for x (a) and y (b) directions related to the uniform and fundamental mode proportional load patterns.

It is worth noticing how the uniform and the fundamental mode proportional load patterns provide similar results in terms of the capacity curve. In this case study, the fundamental mode proportional load pattern is assumed as a reference pattern since it leads to more conservative results. The N2 method (Fajfar and Gašperšič 1996) has been adopted to convert the structure in an equivalent Single Degree Of Freedom (SDOF). A bilinearization of the capacity curve is performed to obtain the equivalent elastic strength and displacement parameters, while the equivalent mass is given by Eq. (5).

$$m^* = \{\phi\}^T [M] \{i\} \tag{5}$$

where *[M]* is the mass matrix of the building and $\{\phi\}$ is the shape vector proportional to the assumed load pattern. The stiffness of the equivalent SDOF is calculated as the ratio between the base shear and top displacement associated with the yield point of the bilinear capacity curve. According to the NTC2018 (NTC 2018) the performance point is assessed through an iterative procedure where the seismic demand is scaled based on the equivalent viscous damping. Furthermore, the maximum base shear obtained from pushover analysis has been considered as the maximum seismic force that can be supported by the structure ($F^*_{collapse}$).

Results show that the maximum force bearing capacities are 9401 kN and 7586 kN for x and y directions, respectively. Figure 13 shows the performance points of the building for both x and y directions. It illustrates that the building has almost the same yielding strengths in both directions, while it reaches the yielding point earlier in the x-direction (d^*_y =3.9 cm) in comparison to the y-direction (d^*_y =7.3 cm). However, the building results more ductile in the x-direction (μ_x =2.13) with respect to the y-direction (μ_y =1.58). Figure 14 shows the plastic hinges distribution at collapse for both x and y directions and the level of axial strain exceeding the elastic threshold (ε_y) in the RC shear walls.

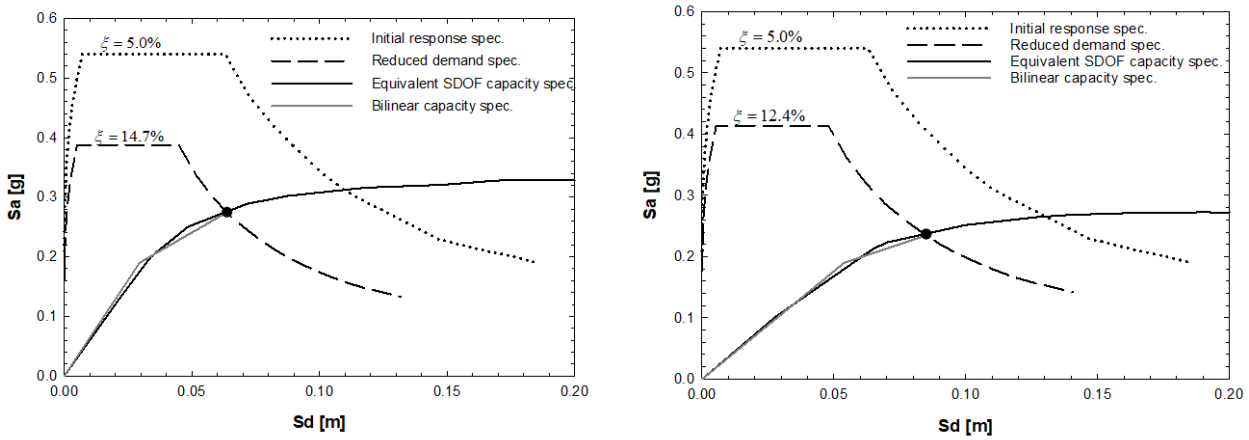

Figure 13 Performance point for x (a) and y (b) directions related to the fundamental mode proportional load patterns.

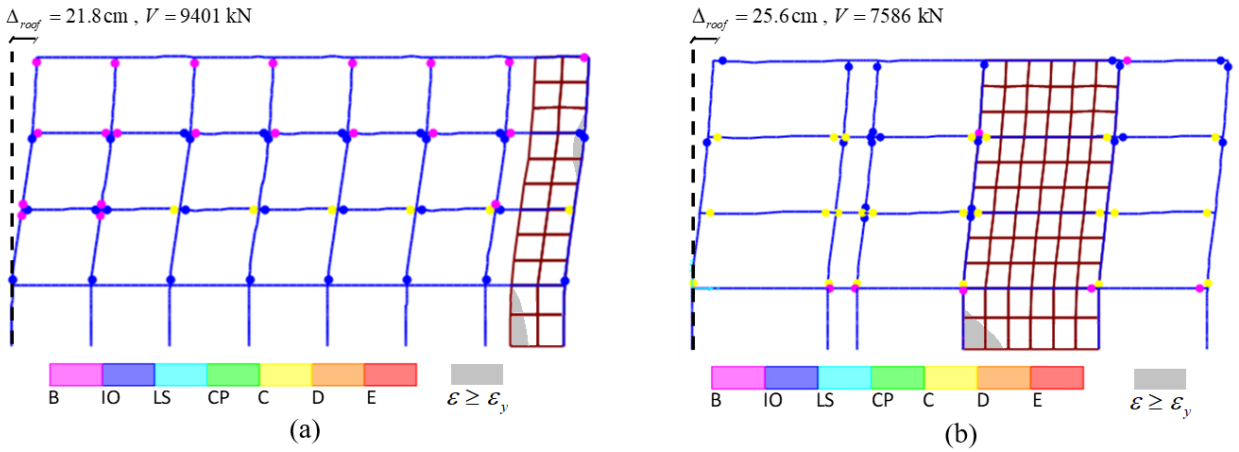

Figure 14 Plastic hinges formation at collapse for the x-direction (frame_A) (a) and the y-direction (frame_B) (b) related to the fundamental mode proportional load patterns.

Vulnerability indices have been computed using Equation (3), and Table 4 reports the performance points and the associated vulnerability indices. The result shows that the building is slightly more vulnerable in the y-direction

(ζ_y =1.13) in comparison to the x-direction (ζ_x =1.19). This is coherent with the distribution of the plastic hinges developed in the y-direction, where a soft-story mechanism is observed on the third floor (Figure 14.b).

Table 4 Performance point characteristics and vulnerability indices computed using Method #3.

Dir.	Equiv. damping	Spectrum reduction	Yielding point				Performance point				Max. base shear	Vulner. index
	x_{eq} [%]	η_{eq}	S_{d_y} [m]	S_{a_y} [g]	d^*_y [m]	F^*_y [kN]	S_{d_max} [m]	S_{a_max} [g]	d^*_{max} [m]	F^*_{max} [kN]	$F^*_{collapse}$ [kN]	ζ_E
x	14.7	0.71	0.029	0.193	0.039	5510	0.063	0.273	0.083	7917	9401	1.19
y	12.4	0.76	0.054	0.189	0.073	5427	0.085	0.235	0.115	6712	7586	1.13

Results - First Level method

The first level method proposed by Islam et al. (2017) has been herein used to assess the vulnerability index of the case study building based on simple information associated with the geometry and strength of the structural members as given by Eq. (6).

$$\zeta_E = \frac{\tau_c \cdot \frac{\sum A_{RC,col}}{\sum A_{floor}} + \tau_m \cdot \frac{\sum A_{wall}}{\sum A_{floor}}}{\frac{W}{\sum A_{floor}} \cdot S_a(T_{ref}) \cdot D_s} \tag{6}$$

where τ_c and τ_m are the shear strength of RC columns and walls, respectively, set equal to $1/6 \cdot \sqrt{f_c}$. Furthermore, $\sum A_{RC,col}$, $\sum A_{wall}$, and $\sum A_{floor}$ represent the total area of the RC columns, walls, and floor, respectively. The weight of the building per unit area is defined by the term $W / \sum A_{floor}$, while D_s is a threshold assumed to be 3/5 for inelastic range, and 1 for elastic range. The three area parameters have been computed from the building's drawings and the total weight has been derived based on the available information about the materials from the BIM model. The spectral acceleration at the fundamental period of the buildings has been assumed as the maximum value between the spectral accelerations associated with the performance points (scaled design spectrum) obtained through pushover analysis (Table 4). This assumption implies that the D_s coefficient is equal to 1. In case that pushover results are not available, the spectral acceleration at the reference period may be evaluated as the spectral acceleration of the target spectrum associated with the elastic first mode period assessed through the simplified formulation proposed by the NTC2018 (NTC2018 2018).

Table 5 summarizes the building's parameters and the related vulnerability index evaluated with Eq. (6).

Table 5 Building's parameters and vulnerability index according to Islam et al. (2017)

$\Sigma A_{RC,col}$ [m^2]	ΣA_{wall} [m^2]	ΣA_{floor} [m^2]	τ_c [MPa]	τ_m [MPa]	W [kN]	$Sa(T_{ref})$ [g]	D_s [-]	ζ_E
7.200	22.680	994.560	0.935	0.935	10205.324	0.273	1.000	1.02

Results - Second Level method

The simplified method proposed by Thermou and Pantazopoulou (2011) has been adopted as a second-level procedure for assessing the vulnerability index of the case study building. The index is computed as the ratio between the average inter-story drift at the collapse $\theta_{failure}$ and the drift demand θ_d at the considered limit state. The first quantity is evaluated as given by Eq. (7).

$$\theta_{failure,i} = \theta_{y,i} \cdot \frac{V_{Rd,tot,i}}{V_{y,tot,i}} \tag{7}$$

where $\theta_{y,i}$ is the inter-story drift at i^{th} column yielding that can be assessed based on the cantilever model based on the steel strain at yield and the column depth, while $V_{Rd,tot,i}$ and $V_{y,tot,i}$ are the total shear strength of the columns and the total shear force required to develop flexural yielding (Thermou and Pantazopoulou 2011). The i^{th} drift demand is computed approximating the fundamental response shape through a sinusoidal function(Gulkan and Sozen 1999) as given by Eq. (8).

$$\theta_{d,i} = \frac{1.216 \cdot a_g \cdot \left(n^2 \cdot Q_1^2\right)_i}{h_i} \cdot \sin\left(\pi / 2 \cdot n\right) \quad \left[0.15 \le T \le 0.50\right] \tag{8}$$

where a_g is the maximum ground acceleration associated with the LSC considered limit state and n is the number of stories. The coefficient Q_i takes into account the floor area ratios of the vertical members for dual systems (Thermou and Pantazopoulou 2011). Based on the BIM model and the dynamic characterization of the building, the structural coefficients and the associated vulnerability index are listed in Table 6.

Table 6 Building's parameters and vulnerability index according to Thermou and Pantazopoulou (2011)

$V_{y,tot}$ [kN]	$V_{RD,tot}$ [kN]	θ_y [%]	$\theta_{failure}$ [%]	θ_d [%]	ζ_E
94.09	68.72	0.59	0.44	0.39	1.14

COMPARISONS AND DISCUSSION

Comparisons among different GMSM

The vulnerability indices obtained with Methods #1 and #2 assume different values compared the adopted ground motion selection procedures. Even if a detailed comparison of the GMSM approaches is out of the scope of this article, the following discussion is meant to investigate the variability range of the estimated vulnerability indices and the influence of the adopted GMSM. Therefore, the dynamic response dispersion $\beta_{collapse}$ around the mean values of the $PGA_{collapse}$ and the Sa for Method #1 and #2, respectively, has been analyzed.

Following the Table 2 results, the variability of the computed PGA at the collapse limit is found to be slightly lower when the first record selection (Marasco and Cimellaro 2018) is adopted. Similar results have been obtained when Method #2 is applied (Table 3). In this case, the standard deviation of the spectral acceleration at collapse ranged from 0.04 g to 0.08 g. The second record selection approach(Iervolino, Galasso, and Cosenza 2010) provides higher values of dispersion, while almost the same standard deviation values have been found using first (Marasco and Cimellaro 2018) and third (Hachem 2008) selection. Moreover, the dynamic response dispersion has been found always higher when the 2% drift limit is assumed.

In parallel with the assessment of the standard deviation for the dynamic response, the maximum and minimum values of both $PGA_{collapse}$ and Sa have been also evaluated. These parameters provide a measure of the absolute maximum dispersion associated with each GMSM procedure (Figure 15).

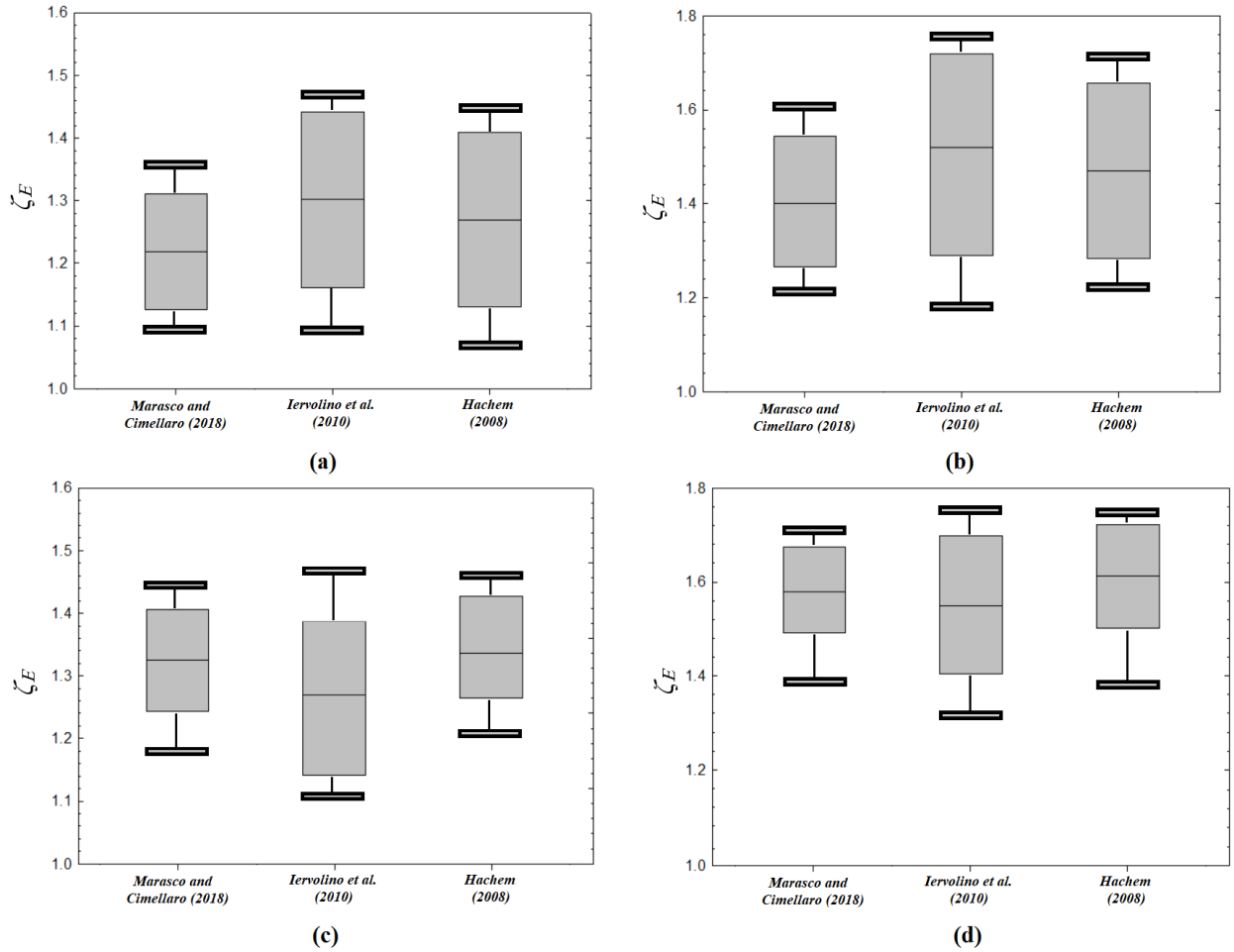

Figure 15 Mean vulnerability index for 0.8% drift limit ratio (a) and 2% drift limit ratio (b), and mean spectral acceleration at collapse for 0.8% drift limit ratio (c) and 2% drift limit ratio (d), with related maximum range of variability and associated 68% confidence level.

The boxes midline represent the mean vulnerability index ζ_E, while the grey area refers to the range of values within the interval $\zeta_E \pm \beta_{collapse} / PGA_{design}$ and $\zeta_E \pm \beta_{collapse} / S_{a,d}$ for Method #1 and #2, respectively. Furthermore, the black whiskers represent the absolute maximum and minimum dynamic responses for a given set of motions.

Figure 15 highlights how the confidence level and the extreme values associated with the second (Iervolino, Galasso, and Cosenza 2010) and third(Hachem 2008) selections spread on a wider band with respect to the first one (Marasco and Cimellaro 2018). It is also worth noting how the confidence levels and the maximum and minimum dispersions obtained with the second (Iervolino, Galasso, and Cosenza 2010) and third (Hachem 2008) selections for Method #1 are considerably higher than those achieved with the first one(Marasco and Cimellaro 2018). This discrepancy lies in the formulation of the first GMSM procedure(Marasco and Cimellaro 2018), where the records are selected to match the target spectrum within the reference range of period and also to have a reduced dispersion of the PGA. Limiting the variability of the PGA of the selected motions leads to produce values of $PGA_{collapse}$ with low dispersion around its mean. Thus, according to Eq. (1), the vulnerability index shows a reduced standard deviation and maximum absolute dispersion. In the remaining of the paper, first GMSM procedure (Marasco and Cimellaro 2018) has been adopted as the reference one.

Comparisons among the three proposed methods

As an attempt to emphasize the main differences among the three proposed methods, the results based on the reference GMSM procedure(Marasco and Cimellaro 2018) have been herein considered. The results from Methods #1 and #2 confirm that the selection of the time histories and the scaling procedure can significantly affect the vulnerability assessment when dynamic nonlinear analyses are used. Method #1 is simpler to be implemented in comparison to Method #2, but its scaling procedure to the same peak ground acceleration affects the spectrum matching between the selected ground motion records and the design spectrum.

The seismic input energy during time has been calculated as the integral of the base shear over the ground displacement. The base shear is given by the product between the building mass and the sum of the ground and floor accelerations. Figure 16 depicts the average seismic input energy for the sets of scaled ground motions used in Method #1 and Method #2. It shows that the input energy for Method #1 is higher for both collapse drift limits. Indeed, the scaling procedure of Method #2 assumes the input energy provided by the selected scaled records is equivalent to the energy of the scaled design spectrum. On the contrary, the ground motions of Method #1 transfer a higher amount of energy by simply scaling the records. This leads to developing a higher damage level and, consequently, to a vulnerability index underestimation. The result shows that Method #1 underestimates the vulnerability indices of about 8.3% and 12.1% less than Method #2 for 0.8% and 2% drift limits, respectively.

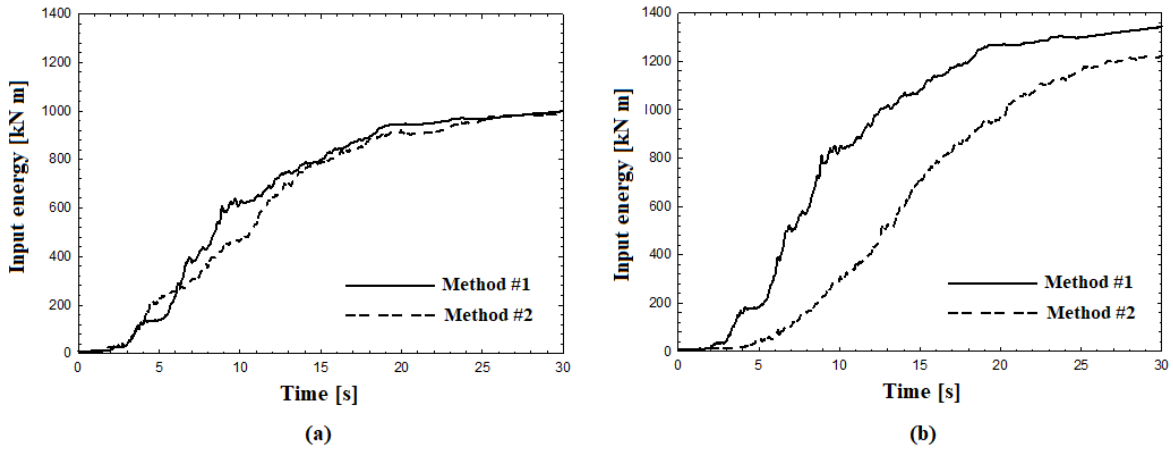

Figure 16 Average input energy for the seven selected time histories at the collapse state; for 0.8% drift limit ratio (Ghobarah 2004) (a) and 2% drift limit ratio (FEMA 273) (b).

Method #3 evaluates the building vulnerability assuming that the structural response is controlled by a single-mode that remains constant throughout the time history response. Furthermore, the roof drift that is associated with the level of damage is a global measure of the overall structural deformation and does not reflect the damage distribution along with the building height. Method #3 evaluates a lower value of the vulnerability index (ζ =1.13) with respect to the dynamic methods.

The drift at the performance point has been computed and compared with the two bearable maximum drifts selected (0.8% and 2%). The maximum displacement at the performance point for the equivalent SDOF system is d^*_{max} = 0.115 m, and the corresponding drift is 0.84%. This value is equivalent to the drift limit of 0.8% used for Method #1 and Method #2 that corresponds to non-ductile behavior, as confirmed by the low ductility value (μ =1.58) determined by the pushover analysis.

The vulnerability index using Method #3 is reasonably similar to those computed using the dynamic methods and assuming the maximum drift limit to 0.8%. In particular, the vulnerability index computed with Method #3 is 7% and 16% lower than those from Method #1 and Method #2, respectively. Instead, assuming a drift limit of 2% in the dynamic analyses, Method #3 would lead to less accurate results (25% less than Method #1 and 40% less than Method #2). These discrepancies are partially due to the type of analyses used to assess the vulnerability index. Indeed, (Causevic and Mitrovic 2011) demonstrated that the maximum dynamic response reached with nonlinear time history analysis will be greater than those obtained through nonlinear static analysis.

Table 7 summarizes the different characteristics of the proposed methods, applied to the considered case study. Method #1 and Method #3 results more conservative than Method #2, which is more computationally demanding.

Table 7 Comparison between different proposed methods characteristics.

	Type of analysis	Modeling effort demand [s]	Total computational effort	The necessity to select a drift limit	n° of analyses to reach collapse threshold	Level of detail
Method #1	NL-Dynamic	*187.32	Medium	Yes	21 (7 x 3)	Medium
Method #2	NL-Dynamic		High	Yes	35 (7 x 5)	High
Method #3	NL-Static	24.26	Low	No	–	Low

* Average value based on the 7 pair of selected time history

Comparisons among the three level-based methods

The vulnerability indices identified by using accurate nonlinear analyses based on the three proposed methods have been compared with those achieved through a first and second-level approach (Figure 17). The results based on the reference GMSM procedure have been here considered for Method #1 and #2, while the minimum value between x and y directions associated with Method #3 (pushover-based analysis) has been assumed for comparison.

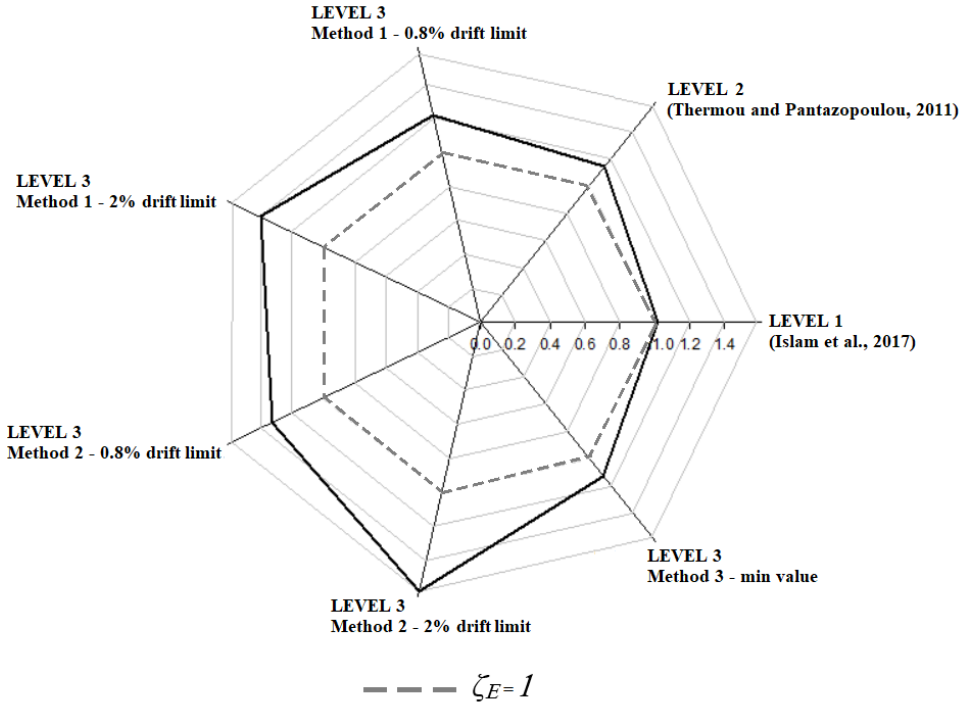

Figure 17 Vulnerability index associated with Level 1(Islam et al. 2017), 2(Thermou and Pantazopoulou 2011), and 3 (Method #1-2-3) procedures.

The case study building has been found safe ($\zeta_E > 1$) by applying the considered procedures and vulnerability indices. The safety level against the collapse assumes a lower value when the first-level procedure is carried out. On the contrary, comparable results have been achieved for the second-level approach and Method #3 that could be considered at the equivalent level of detail with respect to second-level procedures by using simplified static nonlinear analyses. Finally, Methods #1 and #2 based on engineering analysis with a higher level of detail provide the highest values of vulnerability indices. Therefore, coherently with the type of analysis performed, the variability

of the obtained results lies in their level of detail and the building parameters used to assess vulnerability. The first and second-level methodologies provided lower values of vulnerability index than those obtained with the third level because they are not capable of accounting for the nonlinear behavior. These results may be explained by the ductile capacity of the case study building. The investigated building exhibits a remarkable ductile behavior which is satisfactorily taken into account by the refined FEM model. Differently, the system ductility is not adequately considered in the first and second-level methodologies.

Indeed, the first-level method aims at identifying the global building capacity based on the shear strength of the members and their resistant area. Therefore, this force-based method attempts to assess the building capacity assuming a shear-based resistant mechanism while defining the seismic demand as proportional to the building mass. Although this model provides a rapid vulnerability assessment, it neglects the building ductility that can be taken into account by using a displacement-based approach. Therefore, it leads to underestimating the vulnerability index of the building.

The second-level method provides an estimate of the building vulnerability based on its drift capacity. Many authors revealed how drift is a feasible EDP in predicting building damage(Krawinkler, Medina, and Alavi 2003). Furthermore, the drift demand and capacity have been evaluated by assuming a limited set of characteristics building parameters such as the floor area ratio of vertical members and the cross-section sizes of the resisting frame members. Similarly to Method #3, the seismic demand is meant as the maximum action or drift expected on the structure, while the deformed shape is assumed to be proportional to a given mode. Such kind of input modeling does not consider the real dynamic variability of the seismic excitation neglecting the effects of higher frequency modes. To overcome this limitation, Methods #1 and #2 are proposed to assess the building vulnerability through nonlinear time history analyses. The dynamic nonlinear analyses (Methods #1 and #2) leads to obtain a higher estimate of the maximum displacement capacity with respect to those achieved by the nonlinear simplified procedure.

Generally, the first and second-level methods do not provide accurate results for individual building-scale applications. They are currently employed as low computational demanding methods for medium or large-scale applications. To improve their level of detail, first and second-level methods may be calibrated based on the results obtained with third-level analyses.

CONCLUDING REMARKS

This paper presents three different vulnerability assessment methods at collapse limit state using nonlinear dynamic analysis (Method #1 and Method #2) and pushover analysis (Method #3) providing different vulnerability indices. The ground motion selection has been conducted comparing three different approaches from the literature. A reinforced concrete building has been used as a case study to compare the results selecting different sets of drifts associated with the collapse limit states. Furthermore, first and second-level methodologies from the literature have been also applied and compared with the three proposed methods. The results show that the ground motions selection and the scaling procedure affect the computation of the vulnerability indices. Indeed, limiting the dynamic response dispersion leads to reduce the confidence interval range of the estimated vulnerability index.

Method #1 is simpler to apply than Method #2 and requires less computational effort using the scaling procedure based on PGA. Whereas, Method #2 is more computationally demanding because it requires the selection of a new set of spectrum compatible ground motions at each iteration, and provides higher index values with respect to Method #1. However, Method #2 allows limiting the distortion of the energy content in the generated records. Furthermore, the vulnerability index estimates by both Method #1 and #2 have shown a strong correlation with the limit states definition.
Method #3 is based on nonlinear static analyses, therefore it is faster to be applied, but it can underestimate the vulnerability index for high ductile buildings considering a force-based approach. Method #3 could be used as a preliminary vulnerability assessment method for non-ductile structures when the dynamic response is dominated by the first mode. It is also worth noticing that Method #3 can be misleading when applied to structures with a capacity curve that highlights an elastic-perfectly plastic behaviour or if the collapse belongs to a softening branch.
Further developments may focus on a coherent comparison between force-based and displacement-based approaches to compute vulnerability indices using the same method of analysis. In particular, Method #3 could specifically lend

itself to this comparison, although with its inherent limitations (e.g., building regularity, predominant first mode) of using a static method to describe typically dynamic phenomena.

The results provided by the First and Second Level methods revealed that the case study building can be considered safe. Furthermore, the safety margin against the collapse is lower when the First Level procedure is carried out and increases with the Second Level procedure. These simplified methods allow a precautionary estimation of the vulnerability index, even if only with more accurate approaches, such as those proposed, a more realistic level of vulnerability can be defined.

ACKNOWLEDGMENTS

The research leading to these results has received funding from the European Research Council under the Grant Agreement n° ERC_IDEAL RESCUE_637842 of the project IDEAL RESCUE - Integrated Design and Control of Sustainable Communities During Emergencies. Furthermore, the authors would like to thank the Municipality of Melzo (Italy) in which the school building belongs as well as Dr. V. Villa (Politecnico di Torino) for her endless support and providing the BIM model. Prof. Farhad Ansari (University of Illinois at Chicago) is also gratefully acknowledged for his expert support to the on-site investigations and his helpful suggestions. The cooperation of the doctoral students and post-docs of the Resilience Lab at the Politecnico di Torino – DISEG for the on-site investigations is also acknowledged.

REFERENCES

Adam, Christoph, Styliani Tsantaki, Luis F Ibarra, and David Kampenhuber. 2014. Record-to-record variability of the collapse capacity of multi-story frame structures vulnerable to P-delta. Paper read at Proceedings of the second European conference on earthquake engineering and seismology (2ECEES).

Al-Chaar, Ghassan. 2002. Evaluating strength and stiffness of unreinforced masonry infill structures: ENGINEER RESEARCH AND DEVELOPMENT CENTER CHAMPAIGN IL CONSTRUCTION ….

Al-Chaar, Ghassan, Mohsen Issa, and Steve Sweeney. 2002. Behavior of masonry-infilled nonductile reinforced concrete frames. *Journal of Structural Engineering* 128 (8):1055-1063.

Alam, N, M Shahria Alam, and S Tesfamariam. 2012. Buildings' seismic vulnerability assessment methods: a comparative study. *Natural hazards* 62 (2):405-424.

ASCE-7. 2014. Seismic evaluation and retrofit of existing buildings: American Society of Civil Engineers Reston, VA.

Asteris, Panagiotis G, MP Chronopoulos, CZ Chrysostomou, H Varum, V Plevris, Nicholas Kyriakides, and V Silva. 2014. Seismic vulnerability assessment of historical masonry structural systems. *Engineering Structures* 62:118-134.

ATC-21. 1988. Rapid visual screening of buildings for potential seismic hazards: A handbook. Applied Technology Council, Redwood city, CA, USA: Government Printing Office.

ATC-40. 1996. Seismic evaluation and retrofit of concrete buildings. 2. Appendices. Redwood City,California: Applied Technology Council.

Bertogg, Martin, Luzi Hitz, and Edouard Schmid. 2002. Vulnerability functions derived from loss data for insurance risk modelling: findings from recent earthquakes. Paper read at Proceedings of the twelfth European conference on earthquake engineering (paper 281), London.

Calvi, G Michele, Rui Pinho, Guido Magenes, Julian J Bommer, L Fernando Restrepo-Vélez, and Helen Crowley. 2006. Development of seismic vulnerability assessment methodologies over the past 30 years. *ISET journal of Earthquake Technology* 43 (3):75-104.

Calvi, GM, MJN Priestley, and MJ Kowalsky. 2007. Displacement based seismic design of structures. Paper read at New Zealand Conference on Earthquake Engineering.

Causevic, Mehmed, and Sasa Mitrovic. 2011. Comparison between non-linear dynamic and static seismic analysis of structures according to European and US provisions. *Bulletin of earthquake engineering* 9 (2):467-489.

Chácara, César, Francesco Cannizzaro, Bartolomeo Pantò, Ivo Caliò, and Paulo B Lourenço. 2019. Seismic vulnerability of URM structures based on a Discrete Macro-Element Modeling (DMEM) approach. *Engineering Structures* 201:109715.

Chieffo, Nicola, Francesco Clementi, Antonio Formisano, and Stefano Lenci. 2019. Comparative fragility methods for seismic assessment of masonry buildings located in Muccia (Italy). *Journal of Building Engineering*:100813.

Cimellaro, Gian Paolo, and Sebastiano Marasco. 2015. A computer-based environment for processing and selection of seismic ground motion records: OPENSIGNAL. *Frontiers in Built Environment* 1:17.

Cimellaro, Gian Paolo, S Piantà, and A De Stefano. 2012. Output-only modal identification of ancient L'Aquila city hall and civic tower. *Journal of structural engineering* 138 (4):481-491.

CIRCOLARE. 2019. 21 gennaio 2019, n. 7 CS LL. PP. Istruzioni per l'applicazione dell'Aggiornamento delle "Norme tecniche per le costruzioni", di cui al decreto ministeriale 17 gennaio 2018.

Cockburn, G, and S Tesfamariam. 2012. Earthquake disaster risk index for Canadian cities using Bayesian belief networks. *Georisk: Assessment and Management of Risk for Engineered Systems and Geohazards* 6 (2):128-140.

Colombini, STEFANO. 2014. Vulnerabilità sismica di edifici esistenti in cemento armato e in muratura. *Roma: EPC Editore*.

CSI. 2018. Integrated finite element analysis and design of structures basic analysis reference manual. *Computers and Structures Inc, Berkeley (CA, USA)*.

Djemai, MC, M Bensaibi, and K Zellat. 2019. Seismic vulnerability assessment of bridges using analytical hierarchy process. Paper read at IOP Conference Series: Materials Science and Engineering.

El Khoudri, M, L Ben Allal, Mahjoub Himi, and D El Adak. 2016. Evaluation de la vulnérabilité sismique des bâtiments en béton arméen utilisant l'analyse dynamique incrémentale (Seismic vulnerability assessment of reinforced concrete buildings using Incremental Dynamic Analysis IDA). *Journal of Materials and Environmental Science, 2016, vol. 7, num. 2, p. 481-487*.

Emami, Ali R, and Amir M Halabian. 2017. Incremental dynamic collapse analysis of RC core-wall tall buildings considering spatial seismic response distributions. *The Structural Design of Tall and Special Buildings* 26 (15):e1383.

Eurocode-8. 2005. Design of structures for earthquake resistance-part 1: general rules, seismic actions and rules for buildings. In *Brussels: European Committee for Standardization (EN 1998–1)*.

Fajfar, Peter, and Peter Gašperšič. 1996. The N2 method for the seismic damage analysis of RC buildings. *Earthquake engineering & structural dynamics* 25 (1):31-46.

FEMA154. 2002. *Rapid visual screening of buildings for potential seismic hazards: A handbook*. Edited by G. P. O. Federal Emergency Management Agency. 2, ATC 154 (originally published in 1988), ed. Washington, DC

FEMA273. 1997. NEHRP guidelines for the seismic rehabilitation of buildings: Federal Emergency Management Agency Washnigton, DC.

FEMA310. 1998. Handbook for the Seismic Evaluation of Buildings: A Prestandard. Washington, DC: Federal Emergency Management Agency.

FEMA356, FEDERAL EMERGENCY MANAGEMENT AGENCY -. 2000. Prestandard and Commentary for the Seismic Rehabilitation of Buildings. Washington DC.

FEMA1999. 1999. Earthquake Loss Estimation Methodology: User's Manual HAZUS 99. *Federal Emergency Management Agency, Washington, DC*.

Formisano, A, and A Marzo. 2017. Simplified and refined methods for seismic vulnerability assessment and retrofitting of an Italian cultural heritage masonry building. *Computers & Structures* 180:13-26.

Gentile, Roberto, Carmine Galasso, Yunita Idris, Ibnu Rusydy, and Ella Meilianda. 2019. From rapid visual survey to multi-hazard risk prioritisation and numerical fragility of school buildings. *Natural Hazards and Earth System Sciences Discussions* 19 (7):1365-1386.

Gentile, Roberto, Andrea Nettis, and Domenico Raffaele. 2020. Effectiveness of the displacement-based seismic performance assessment for continuous RC bridges and proposed extensions. *Engineering Structures* 221:110910.

Ghobarah, Ahm. 2004. On drift limits associated with different damage levels. Paper read at International workshop on performance-based seismic design.

Giordano, Nicola, Flavia De Luca, and Anastasios Sextos. 2020. Out-of-plane closed-form solution for the seismic assessment of unreinforced masonry schools in Nepal. *Engineering Structures* 203:109548.

Guéguen, Philippe, Clotaire Michel, and Laele LeCorre. 2007. A simplified approach for vulnerability assessment in moderate-to-low seismic hazard regions: application to Grenoble (France). *Bulletin of Earthquake Engineering* 5 (3):467-490.

Gulkan, Polat, and Mete A Sozen. 1999. Procedure for determining seismic vulnerability of building structures. *Structural Journal* 96 (3):336-342.

Hachem, Mahmoud M. 2008. QuakeManager: A software framework for ground motion record management, selection, analysis and modification. Paper read at Proceeding of 14th World Conference on Earthquake Engineering WCEE, Beijing, October.

Harirchian, Ehsan, and Tom Lahmer. 2019. Earthquake Hazard Safety Assessment of Buildings via Smartphone App: A Comparative Study. Paper read at IOP Conference Series: Materials Science and Engineering.

Hill, Marc, and Tiziana Rossetto. 2008. Comparison of building damage scales and damage descriptions for use in earthquake loss modelling in Europe. *Bulletin of Earthquake Engineering* 6 (2):335-365.

Iervolino, Iunio, Carmine Galasso, and Edoardo Cosenza. 2010. REXEL: computer aided record selection for code-based seismic structural analysis. *Bulletin of Earthquake Engineering* 8 (2):339-362.

Islam, Md Shafiul, Hamood Alwashali, Yuta Torihata, Kiwoong Jin, and M Maeda. 2017. Rapid seismic capacity evaluation method of RC buildings with masonry infill. *Architectural Institute of Japan-Academic Lecture Collection Summary*:195-196.

Jain, Sudhir K, Keya Mitra, Manish Kumar, and Mehul Shah. 2010. A proposed rapid visual screening procedure for seismic evaluation of RC-frame buildings in India. *Earthquake Spectra* 26 (3):709-729.

Kassem, Moustafa Moffed, Fadzli Mohamed Nazri, and Ehsan Noroozinejad Farsangi. 2019. Development of seismic vulnerability index methodology for reinforced concrete buildings based on nonlinear parametric analyses. *MethodsX* 6:199-211.

Khan, Sibghat Ullah, Muhammad Irshad Qureshi, Irfan Ahmad Rana, and Ahsen Maqsoom. 2019. An empirical relationship between seismic risk perception and physical vulnerability: a case study of Malakand, Pakistan. *International Journal of Disaster Risk Reduction* 41:101317.

Krawinkler, Helmut, Ricardo Medina, and Babak Alavi. 2003. Seismic drift and ductility demands and their dependence on ground motions. *Engineering structures* 25 (5):637-653.

Lang, Kerstin, and Hugo Bachmann. 2004. On the seismic vulnerability of existing buildings: a case study of the city of Basel. *Earthquake Spectra* 20 (1):43-66.

Lorenzoni, Filippo, Maria Rosa Valluzzi, and Claudio Modena. 2019. Seismic assessment and numerical modelling of the Sarno Baths, Pompeii. *Journal of Cultural Heritage* 40:288-298.

Marasco, S, and GP Cimellaro. 2017. A new energetic based ground motion selection and modification algorithm. Paper read at Proceedings of 16th World Conference on Earthquake Engineering, 16WCEE, Paper.

Marasco, S, and GP Cimellaro. 2018. A new energy-based ground motion selection and modification method limiting the dynamic response dispersion and preserving the median demand. *Bulletin of Earthquake Engineering* 16 (2):561-581.

Martinelli, A, G Cifani, G Cialone, L Corazza, A Petracca, and G Petrucci. 2008. Building vulnerability assessment and damage scenarios in Celano (Italy) using a quick survey data-based methodology. *Soil Dynamics and Earthquake Engineering* 28 (10-11):875-889.

MATLAB. 2017. 9.3. 0 (R2017b). *The MathWorks Inc, Natick, Massachusetts*.

Naeim, Farzad, Hussain Bhatia, and Roy M Lobo. 2001. Performance based seismic engineering. In *The Seismic Design Handbook*: Springer.

Noori, A Zamani, S Marasco, O Kammouh, M Domaneschi, and GP Cimellaro. 2017. Smart cities to improve resilience of communities. Paper read at 8th International Conference on Structural Health Monitoring of Intelligent Infrastructure.

NRCC36943. 1993. Manual for screening of buildings for seismic investigation. Ottawa, Canada: Institute for Research in Construction, National Research Council of Canada.

NTC2018. 2018. Aggiornamento delle Norme Tecniche per le Costruzioni: Updating of the Technical standards for construction. In *Gazzetta Ufficiale*. Italy: Ministero delle Infrastrutture e dei Trasporti.

NTC, D. Min. Infrastrutture e Trasporti 17 gennaio 2018 -. 2018. Norme tecniche per le costruzioni NTC2018

NZSEE-2003. 2014. Assessment and Improvement of the Structural Performance of Buildings in Earthquakes: Prioritisation, Initial Evaluation, Detailed Assessment, Improvement Measures: Recommendations of a NZSEE Study Group on Earthquake Risk Buildings: New Zealand Society for Earthquake Engineering.

NZSEE. 2017. The seismic assessment of existing buildings: Technical guidelines for engineering assessments. *Part C-Detailed Seismic Assessment. Part C8-Unreinforced Masonry Buildings*.

Okada, Shigeyuki, and Nobuo Takai. 2000. Classifications of structural types and damage patterns of buildings for earthquake field investigation. Paper read at Proceedings of the 12th world conference on earthquake engineering (paper 0705), Auckland.

Perrone, Daniele, Maria Antonietta Aiello, Marisa Pecce, and Fernando Rossi. 2015. Rapid visual screening for seismic evaluation of RC hospital buildings. Paper read at Structures.

Ruggieri, Sergio, Daniele Perrone, Marianovella Leone, Giuseppina Uva, and Maria Antonietta Aiello. 2020. A prioritization RVS methodology for the seismic risk assessment of RC school buildings. *International Journal of Disaster Risk Reduction* 51:101807.

Ruggieri, Sergio, Francesco Porco, Giuseppina Uva, and Dimitrios Vamvatsikos. 2021. Two frugal options to assess class fragility and seismic safety for low-rise reinforced concrete school buildings in Southern Italy. *Bulletin of Earthquake Engineering* 19 (3):1415-1439.

Sinha, Ravi, and Alok Goyal. 2004. A national policy for seismic vulnerability assessment of buildings and procedure for rapid visual screening of buildings for potential seismic vulnerability. *Report to Disaster Management Division, Ministry of Home Affairs, Government of India, Hindistan*.

Spence, Robin, Emily So, Sarah Jenny, Hervé Castella, Michael Ewald, and Edmund Booth. 2008. The Global Earthquake Vulnerability Estimation System (GEVES): an approach for earthquake risk assessment for insurance applications. *Bulletin of Earthquake Engineering* 6 (3):463-483.

Sucuoğlu, Haluk, Ufuk Yazgan, and Ahmet Yakut. 2007. A screening procedure for seismic risk assessment in urban building stocks. *Earthquake Spectra* 23 (2):441-458.

Takeda, Toshikazu, Mete A Sozen, and N Norby Nielsen. 1970. Reinforced concrete response to simulated earthquakes. *Journal of the structural division* 96 (12):2557-2573.

Thermou, GE, and Stavroula J Pantazopoulou. 2011. Assessment indices for the seismic vulnerability of existing RC buildings. *Earthquake engineering & structural dynamics* 40 (3):293-313.

Uma, SR, Rajesh P Dhakal, and Mostafa Nayyerloo. 2014. Evaluation of displacement-based vulnerability assessment methodology using observed damage data from Christchurch. *Earthquake engineering & structural dynamics* 43 (15):2319-2339.

Yakut, Ahmet, Guney Ozcebe, and M Semih Yucemen. 2006. Seismic vulnerability assessment using regional empirical data. *Earthquake engineering & structural dynamics* 35 (10):1187-1202.